Synthesis of Superparamagnetic Polymer−Ferrite Composites Using Surfactant Microstructures

Nagesh S. Kommareddi,[†] Murthy Tata,[†] Vijay T. John,*[,†]
Gary L. McPherson,[‡] and Michael F. Herman[‡]

Department of Chemical Engineering and Department of Chemistry, Tulane University, New Orleans, Louisiana 70118

Young-Sook Lee and Charles J. O'Connor*

Department of Chemistry, University of New Orleans, New Orleans, Louisiana 70148

Joseph A. Akkara and David L. Kaplan

U. S. Army Natick Research, Development and Engineering Center, Natick, Massachussetts 01760

Received October 25, 1994. Revised Manuscript Received January 11, 1996[⊗]

Superparamagnetic microspheres are prepared by incorporating nanometer-sized iron oxide crystals into micron-sized phenolic polymer particles. The synthesis of ferrite particles is conducted in the structured environment of water-in-oil microemulsions (reversed micelles). This is followed by the enzymatic polymerization of *p*-ethylphenol. The polymer precipitates in spherical morphologies and during precipitation incorporates ferrite nanocrystals into the polymeric matrix. SQUID (superconducting quantum interference device) generated magnetic hysteresis loops exhibit zero remanence and coercivity for the ferrite−polymer composite at room temperature, indicating the superparamagnetic nature of the composite. At very low temperatures, hysteretic effects, nonzero remanence, and coercivity are seen. Spin glass behavior is apparent at low temperatures from dc magnetic susceptibility measurements. Thermal and isothermal remanent magnetization measurements confirm the existence of the spin glass state. The composites exhibit blocking temperatures in the range 12.0−27.0 K. TEM micrographs of sectioned composite particles show that the iron oxide component is uniformly distributed in the polymer matrix.

Introduction

There has been growing interest in the synthesis of nanoscale inorganic materials, due to the novel properties exhibited by particles of very small dimensions. Materials such as CdS, TiO_2, γ-Fe_2O_3, and Fe_3O_4 have been widely studied. CdS and TiO_2 nanoparticles make excellent photocatalysts and ferrites are used in magnetic inks,[1] magnetic fluids,[1] magnetic recording.[2] Recently, many researchers have successfully synthesized fine particles exploiting the restricted environments offered by surfactant systems. Water-in-oil (w/o) microemulsions[3] (also known as reversed micelles), liquid crystals,[4] and vesicles[5,6] are examples of such systems used in nanoparticle synthesis. From an applications perspective, these nanoscale materials have to be ultimately fashioned into higher order assemblies such as microspheres, fibers, tubes, and sheets, either during or after synthesis. One such attempt is described by Archibald and Mann[7] where lipid tubules are used to synthesize inorganic iron oxide composites. Ziolo and co-workers[8] have reported on the synthesis of an optically transparent, magnetic, iron oxide−polymer composite material using an ion-exchange resin. More recently, Bunker and co-workers[9] have reported on the biomimetic processing of inorganic−organic composite materials using functionalized interfaces to induce crystal nucleation and growth.

In this article, we describe the synthesis and characterization of a novel inorganic−organic composite material. The model inorganic component is iron oxide and the organic component is the polymer poly(*p*-ethylphenol) (PEP). The ease in processibility of phenolic polymers makes them particularly attractive in the synthesis of composite materials. The composite synthesis described in this article is a generalized one and can be easily extended to other inorganic components in the polymeric matrix.

The preparation of polymer−ferrite nanocomposites as described here evolves from our earlier work on

* To whom correspondence should be addressed.
[†] Department of Chemical Engineering.
[‡] Department of Chemistry.
[⊗] Abstract published in *Advance ACS Abstracts,* February 15, 1996.

(1) Charles, S. W.; Popplewell, J. In *Ferromagnetic Materials*; Wohlfarth, E. P., Ed.; North-Holland: Amsterdam, 1980; Vol. 2, p 509.
(2) Bate, G. *J. Appl. Phys.* **1981**, *52*, 2447.
(3) Petit, C.; Lixon, P.; Pileni, M. P. *J. Phys. Chem.* **1990**, *94*, 1598.
(4) O'Sullivan, E. C.; Patel, R. M.; Ward, A. J. I. *J. Colloid Interface Sci.* **1991**, *146*, 582.
(5) Mann, S.; Hannington, J. *J. Colloid Interface Sci.* **1988**, *122*, 326.
(6) Bhandarkar, S.; Bose, A. *J. Colloid Interface Sci.* **1990**, *139*, 541.
(7) Archibald, D. D.; Mann, S. *Nature* **1993**, *364*, 430.
(8) Ziolo, R. F.; Giannelis, E. P.; Weinstein, B. A.; O'Horo, M. P.; Ganguly, B. N.; Mehrotra, V.; Russell, M. W.; Huffman, D. R. *Science* **1992**, *257*, 219.
(9) Bunker, B. C.; Rieke, P. C.; Tarasevich, B. J.; Campbell, A. A.; Fryxell, G. E.; Graff, G. L.; Song, L.; Liu, J.; Virden, J. W.; McVay, G. L. *Science* **1994**, *264*, 48.

0897-4756/96/2808-0801$12.00/0

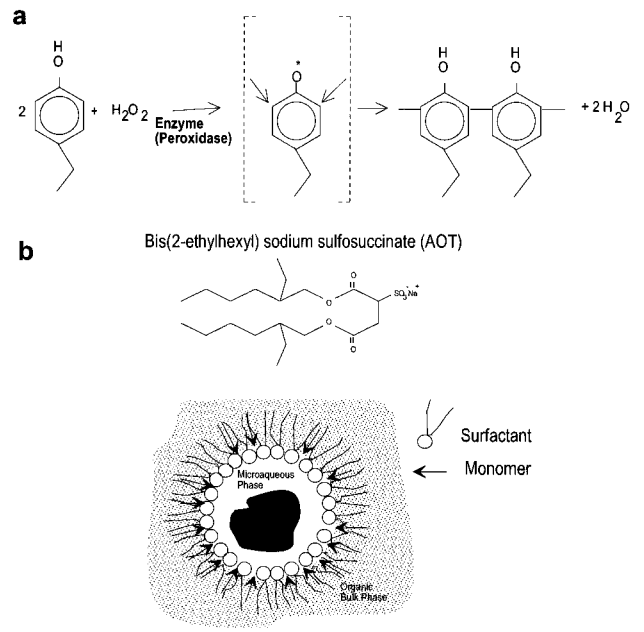

Figure 1. (a) Simplified scheme for the enzyme-catalyzed polymerization reaction of *p*-ethylphenol. The phenoxy radical first formed migrates to the ortho positions, subsequent to which coupling occurs. (b) AOT structure (top) and a representation of the reversed micelle (bottom). The enzyme, depicted by the dark region, resides in the microaqueous phase and the surface-active monomer partitions to the oil−water interface.

phenol polymerization in water-in-oil microemulsions, or reversed micelles as they are often called.[10] Reversed micelles are nanodroplets of water sustained in an organic phase by a surfactant, typically an anionic, bis-(2-ethylhexyl) sodium sulfosuccinate, also referred to as AOT. The water pools of the micelles are capable of solubilizing biomolecules such as enzymes, which retain catalytic activity in what is essentially a minimal water environment. In our earlier work, we found that *p*-alkyl-substituted phenols such as *p*-ethylphenol would partition to the oil−water interface of the micelles. Subsequently, an oxidative enzyme (horseradish peroxidase) encapsulated in the micelles could polymerize the phenols very efficiently to produce polyphenols, which are materials very useful in resins and coatings technologies.[10,11] The reaction is mechanistically analogous to lignin synthesis, and the reaction mechanism and concepts are illustrated in Figure 1a,b.

The remarkable aspect of polymerization in this media is the fact that the polymer formed precipitates out from solution with the morphology of interconnected, submicron-sized spheres. While the full explanation of morphology development is as yet unclear, we do have evidence that the micelles have a templating effect, to fold chains as they are formed to the resulting spheres. Perhaps a simplistic explanation is that of polymer chains growing around the micelle interface; collisions of micelles with growing chains result in chain linkages and the formation of interconnected spherical particles. Eventually the local polymer concentration reaches its solubility limit and precipitation occurs.

As a consequence of the observation of polymer precipitation in the form of interconnected spheres, the concept of preparing polymer−nanoparticle composites arose through the argument that the precipitating polymer may also entrap and pull down inorganic clusters present in the micelles. The objective therefore, was to prepare polymer−nanoparticle composites by a two step approach. In the first step, the water pools of the micelles are used to synthesize inorganic compounds whose growth would be restricted to the nanometer size range by the microstructured synthesis environment. In the second step, monomer (*p*-ethylphenol) and enzyme are added to the system, and polymerization is initiated. The question to be answered was whether polymer synthesis in this environment would result in an entrapment of the nanoparticles. In other words, the objective was to realize a sort of ship-in-a-bottle approach to entrapment and encapsulation of nanoparticles in polymeric microspheres.

This paper indicates the feasibility of such an approach, using ferrite particles as the model inorganic compound, synthesized in the micelles. Reversed micelles constitute a microreactor environment to synthesize inorganic particles restricted to the nanometer size range. As shown by Lopez-Quintela and Rivas,[12] ferrite particles synthesized in reversed micelles have sizes approaching the magnetic domain size. Such particles exhibit superparamagnetic properties. In this paper, we show that incorporation of these ferrite particles into the polymer microspheres confers superparamagnetic properties to the composite. Such superparamagnetic polymers find use in developer compositions for reprographic applications.[13] Polymer beads containing superparamagnetic particles have also found commercial application in the field of biotechnology.[14,15] The morphological characterization of the new magnetic composite material described in this paper is presented through transmission and scanning electron micrographs (TEM and SEM). The magnetic properties of the material were determined using a superconducting quantum interference device (SQUID).

Experimental Section

Materials. Reversed micellar solutions were prepared using the anionic surfactant, bis(2-ethylhexyl) sodium sulfosuccinate (AOT) and isooctane (HPLC grade solvent) obtained from Aldrich Chemical Co., Milwaukee, WI. $FeSO_4$ heptahydrate, enzyme peroxidase (type II: from horseradish), and HEPES (*N*-[2-hydroxyethyl]piperazine-*N*′-[2-ethanesulfonic acid]) buffer were purchased from Sigma Chemical Co., St. Louis, MO. Ammonium hydroxide was obtained from EM Science, NJ. Hydrogen peroxide and *p*-ethylphenol were obtained from Aldrich. Doubly distilled and deionized water was used throughout.

Methods. *Synthesis of Ferrite Particles.* Stock solutions of 0.5 M AOT were used in preparing the reversed micellar solutions containing the reactants $FeSO_4$ and NH_4OH. The so-called injection method was used in preparing all reversed micellar solutions. In a typical preparation, a predetermined amount of reactant stock solution was added to the AOT solution to yield the final reversed micellar solution with the

(10) Rao, A. M.; John, V. T.; Gonzalez, R. D.; Akkara, J. A.; Kaplan, D. L. *Biotechnol. Bioeng.* **1993**, *41*, 531.
(11) Karayigitoglu, C. F.; Kommareddi, N. S.; Gonzalez, R. D.; John, V. T.; McPherson, G. L.; Akkara, J. A.; Kaplan, D. L. *Mater. Sci. Eng. C* **1995**, *2*, 165.
(12) Lopez-Quintela, M. A.; Rivas, J. *J. Colloid Interface Sci.* **1993**, *158*, 446.
(13) Ziolo, R. F., Xerox Corp., U.S. Patent 4,474,866, 1984.
(14) Raineri, I.; Moroni, C.; Senn, H. P. *Nucleic Acids Res.* **1991**, *14*, 4010.
(15) Sharma, P.; Lonneborg, A.; Stougaard, P. *Biotechniques* **1993**, *15*, 610.

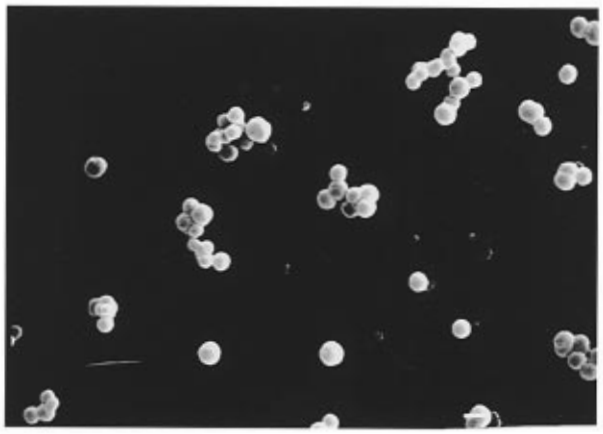

Figure 2. SEM micrograph of the PEP particles synthesized in reversed micelles. The particles are spherical and appear to be fairly monodisperse with particle sizes typically less than 1 μm. The polymer particles exist as single entities or as small clusters.

required w_0 (=[H_2O]/[AOT], molar ratio of water to surfactant) and reactant concentration. For example, to obtain a w_0 10 reversed micellar solution containing $FeSO_4$ at a overall concentration of 0.082 M, 0.45 mL of 0.908 M $FeSO_4$ was added to 5 mL of 0.5 M AOT in isooctane. Separate reversed micellar solutions containing $FeSO_4$ and NH_4OH were prepared by the above procedure. The $FeSO_4$ solutions contained some suspended impurities and had to be centrifuged to obtain clear solutions. The synthesis of ferrite particles was initiated by adding the NH_4OH reversed micellar solution to the $FeSO_4$ reversed micellar solution, while vigorously stirring the mixture. The solution instantly turned bluish-green and within minutes changed to a deep red color. The reaction mixture was kept stirred for about 2 h.

Synthesis of Poly(p-ethylphenol) (PEP) Particles. The simplified mechanism of enzymatic polymerization is shown in Figure 1a. Phenoxy centers migrate to ortho positions where coupling occurs. Our approach is to conduct the polymerization reaction in reversed micelles which solubilize the catalytic enzyme, horseradish peroxidase (HRP). Figure 1b illustrates the structure of the twin-tailed anionic bis(2-ethylhexyl) sodium sulfosuccinate (AOT). Reversed micellar solutions of w_0 (water to surfactant molar ratio) 10 were prepared using 0.01 M HEPES buffer at pH 7.5. In a typical experiment, the enzyme HRP dissolved in HEPES buffer was added to a dry reversed micellar solution, followed by addition of the monomer *p*-ethylphenol (EP). The overall concentration of HRP was kept at 0.5 mg/mL. The enzyme is located in the water core of the reversed micelles, and the amphiphilic monomer partitions to the oil−water interface as shown in Figure 1b, where the arrowhead depicts the polar hydroxyl moiety of the monomer. Evidence for monomer penetration to the interface is seen through shifts in the vibrational frequencies of the surfactant headgroup as a result of hydrogen bonding to the phenolic hydroxyls of the monomer. The reaction of Figure 1a indicates a 1:1 stoichiometry between *p*-ethylphenol reaction and H_2O_2 usage; i.e., for every mole of H_2O_2 added to the reaction mixture, 1 mol of *p*-ethylphenol reacts. Accordingly, the H_2O_2 required for 100% theoretical conversion was calculated. The reaction was initiated by the dropwise addition of the H_2O_2 requirement, in four equal aliquots. The polymerization reaction is extremely rapid, and within minutes of reaction initiation a precipitate is observed. Hydrogen peroxide was added in 30% excess to ensure almost complete conversion of EP. The reaction mixture was normally left to stir overnight. The precipitated polymer was centrifuged and washed extensively with isooctane to remove the surfactant (AOT). The recovered polymer was then oven-dried at 40 °C to remove isooctane and residual water. The morphology of the polymer particles is shown in Figure 2 through a scanning electron micrograph (SEM). As mentioned earlier, the particles are spherical and typically less than 1 μm in diameter. Both individual particles and clusters of spheres are observed. These spherical morphologies are very reproduceably obtained if the AOT to monomer concentrations are kept at a ratio of 3:1 or higher. Further studies of the polymer growth sequence from the micelle scale (0.01 μm) to the observed polymer particle scale (0.2−0.8 μm) are in progress. We just state here that polymer particles can be reproducibly synthesized in spherical morphologies and focus on the preparation of the polymer−ferrite composites and their magnetic property characterizations.

Synthesis of the Ferrite−PEP Composites. Our initial objective was to synthesize polymer in the micellar system directly after synthesis of ferrite particles. However, due to the ferrite synthesis procedure involving NH_4OH addition, the micellar water pools exist at a high pH. The aqueous stock solution corresponding to the same concentration of NH_4OH is at pH 13. At this pH, the ferrite-reversed micellar system is somewhat unstable, with the suspended ferrite particles precipitating out after about 2 days. Additionally, the catalytic enzyme activity is significantly reduced at these high pH levels, as evidenced from the reduced amount of polymer precipitated under these conditions. As a result, it is not feasible to enzymatically synthesize polymer immediately after ferrite synthesis. Rather polymer synthesis has to be conducted only after bringing the water pools to an optimal pH of about 8. Accordingly, after the synthesis of ferrite particles in reversed micelles, 3 mL aliquots were taken and oven-dried overnight at 40 °C to remove NH_4OH from the system. The dried material was then reconstituted to the same volume as the original aliquot by adding isooctane. The final solution is a clear deep-red solution containing ferrite particles sustained in a waterless microemulsion. To this solution, 2 mL of 0.5 M AOT/isooctane solution was added followed by the addition of 0.01 M HEPES buffer (pH 7.5), the monomer (EP), and the enzyme (HRP in buffer) to make up the final reaction mixture. The final reaction conditions were typically w_0 10, with an AOT concentration of 0.5 M, EP 0.15 M, and 0.5 mg/mL HRP. At this stage, the solution contained stable ferrite particles in reversed micelles with all the ingredients required to carry out the polymerization reaction described in the previous section. Again, the reaction was initiated by the dropwise addition of hydrogen peroxide as described before. The presence of ferrite particles in the system does not seem to affect the efficiency of polymerization. The polymer synthesized by this procedure has a distinctive brown color as opposed to the pale yellow color obtained in the absence of ferrite particles. Additional visual evidence for the entrapment of ferrite particles in the polymer is the loss of deep-red color from the supernatant after completion of the polymerization reaction. The ferrite−PEP composite particles were centrifuged and washed extensively with isooctane and oven-dried at 40 °C for further analysis.

Estimation of Iron Content. A Perkin-Elmer atomic absorption spectrometer, fitted with an Fe lamp, was used to determine iron loadings in the polymer composites. About 2.0 mg of the composite was first dissolved in 1 mL of dimethyl formamide (DMF). To this solution, 20 mL of concentrated HCl was added to ensure that all the ferrite was solubilized. The above solution was diluted with DMF to yield a final concentration of 0.1 mg of composite/mL of solution. The absorption of this solution at 248.3 nm was used to determine the iron concentration from a standard calibration curve. The instrument absorbance was autozeroed using pure DMF. A control DMF solution containing 0.1 mg of PEP/mL (no ferrite present) gave an absorbance value of zero. The iron contents reported are the average of two readings obtained by repeating the above procedure with the same composite sample.

Magnetic Measurements. The magnetic properties of the ferrite−PEP composites were characterized using a Quantum Design, Inc. Model MPMS-5S superconducting (SQUID) susceptometer. Calibration and measurement procedures have been described in detail elsewhere.[16] Typically two types of

(16) O'Connor, C. J. O. *Prog. Inorg. Chem.* **1982**, *29*, 203.

experiments were conducted: magnetic susceptibility (both dc, M/H, and ac dM/dH) as a function of temperature and magnetization as a function of field or temperature. Two different procedures were used for the dc magnetic susceptibility experiments: (i) zero-field cooling, where the sample was slowly cooled in zero field to a temperature of 1.7 K at which the measuring field of 1.0 kG was switched on and the magnetization was measured as a function of temperature, and (ii) field cooling where the field of 1.0 kG was turned on at a temperature well above the superparamagnetic blocking temperature before the sample was cooled to 1.7 K. In the ac magnetic susceptibility experiment, a magnetic field of 1.0 G was oscillated at a frequency of 25 Hz under a static zero field while the temperature was scanned from 1.7 to 50.0 K.

In the remanent magnetization measurement, both thermal remanent magnetization (TRM) and isothermal remanent magnetization (IRM) were obtained as a function of field and temperature. The TRM experiment involves slowly cooling the sample in an applied magnetic field to a measuring temperature below the blocking temperature and then switching off the field and measuring the remanent magnetization after a specified elapsed time of 300 s. On the other hand, IRM data are obtained by cooling the sample to the measurement temperature in zero field, applying a field for a long enough time (300 s) and then switching off the field and measuring the remanent magnetization after an elapsed time of 300 s. Standard M vs H hysteresis loops were also recorded at different temperatures ranging from 2.0 to 300.0 K.

Electron Microscopy. For SEM and TEM analysis the polymer particles were dispersed in isooctane by mild sonication. A drop of the dispersed solution was then placed on a SEM stub, and the solvent evaporated within a few minutes. The stub was then placed in a Polaron SEM coating system with an E6900 vacuum base and plasma-coated with gold with the thickness setting at 20 nm. A JEOL JSM-820 scanning microscope was used at an operating voltage of 15 kV for SEM analysis. For the TEM analysis, a drop of the dispersed polymer solution was placed on a carbon-coated Cu grid (100 mesh) and the grid was left to dry for a few minutes before being transferred into the TEM sample chamber. A Phillips EM 410 electron microscope (equipped with an EDAX RT-11 unit for elemental analysis) was operated at an accelerating voltage of 100 kV for TEM analysis. The ferrite-containing polymer particles were analyzed for particle size using regular and microtoming (LKB 2088 Ultratome V) TEM techniques.

X-ray Diffraction. A Scintag XDS-2000 equipped with a Cu $K\alpha_1$ radiation source and a Si(Li) detector was used to record powder diffraction data. The X-ray tube was operated at 45 kV and 40 mA. A scan rate of 2°/min was employed to scan 2θ from 5° to 75°.

Results and Discussion

Ferrite−PEP composite particles were prepared at three different solution conditions. The ferrite synthesis was carried out in reversed micellar solutions corresponding to w_0 values 5, 10, and 15. These samples were taken to dryness ($w_0 < 1$) as explained earlier, and polymerization reactions were carried out after reconstitution to w_0 10. The ferrite−PEP composites contained the following weight percent iron as determined by atomic absorption; for ferrite particles synthesized at w_0 5 micelles, the composite ferrite content was 4.03%, synthesis in w_0 10 micelles resulted in a composite ferrite content of 4.48%, and synthesis in w_0 15 micelles led to a composite ferrite content of 5.34%. The rationale behind varying the w_0 for ferrite synthesis was to study the effect of changing micellar size on the properties of the magnetic material. Micelle size increases with w_0 in AOT reversed micelles[17] and a direct correlation of the water core radius with w_0, R_0 (in nm) $= 1.15\ w_0$, has been reported in the literature.[18] The size of the water pool also correlates with the size of ferrite particles. Properties exhibited by some of the ferrite−PEP composites are presented next through representative data, and comparisons made with the other unrepresented samples.

Electron Microscopy. Direct-view TEM micrographs of the PEP particles (Figure 3a) are somewhat different from the corresponding micrographs of the ferrite−PEP composites (Figure 3b). The images in Figure 3 are of particles at the lower end of the size range and were deliberately selected for their contrast in surface characteristics. The image of the polymer without any incorporated inorganic material (Figure 3a) shows a rather clear boundary; in contrast the ferrite−PEP composite has an image with a more diffuse boundary (Figure 3b). The observation that incorporation of the inorganic material results in a roughened surface is in general valid. The ferrite−PEP particles are decorated by intensely dark spots, which were determined to be iron particles through elemental analysis (EDAX). Clearly the ferrite−PEP particles are distinct from the pure polymer (PEP) particles. Since the sample is too dense to clearly see the ferrite particles through direct view TEM, cut-section transmission electron microscopy was also done. Figure 3c illustrates the cut-section TEM of the ferrite−PEP composite. The polymer particle appears elongated due to the compressive action of the diamond knife during microtoming. The ferrite particles, indicated by the dark spots, are distributed uniformly throughout the polymer matrix. Particle size analysis shows that the particles are typically smaller than 10 nm. XRD patterns of PEP and the ferrite−PEP composite are illustrated in Figure 4. The broad peak centered around $2\theta = 20°$ is from PEP, indicating the amorphous nature of the polymer. The XRD pattern for the ferrite−PEP composite displays two broad but distinct peaks at 2θ values of 35.63° and 62.93°, which correspond to the two most intense peaks of maghemite, γ-Fe_2O_3.[19] The best fits from computer matching the experimental patterns with the ICDD database were that of γ-Fe_2O_3 (maghemite) and Fe_3O_4 (magnetite), with γ-Fe_2O_3 being the better fit. Since the polymerization process involves the addition of hydrogen peroxide, a strong oxidant,[8] it is reasonable to expect maghemite to be the dominant phase in the ferrite−PEP composite.

Magnetic Properties. To determine the magnetic properties of the ferrite−PEP composite material, a SQUID magnetometer was used. Field-dependent hysteresis loops were generated in the temperature range 2.0−300.0 K for the three samples. Typical trends exhibited by the ferrite−PEP composites are described through the hysteresis loops for the w_0 15 sample recorded at 100.0 and 4.5 K, shown in Figure 5a,b, respectively. The magnetization vs field data at 100.0 K illustrates that the data are perfectly superimposable as the field is cycled between ±50 kG, with the coercivity $H_c = 0$. This lack of hysteresis is characteristic of superparamagnetic particles or some single-domain particles of very small dimensions. The particles have

(17) Zulauf, M.; Eicke, H.-F. *J. Phys. Chem.* **1979**, *83*, 480.

(18) Pileni, M. P.; Zemb, T.; Petit, C. *Chem. Phys. Lett.* **1985**, *118*, 4.

(19) Powder Diffraction File (PDF) 39-1346, from the ICDD Database−International Center for Diffraction Data, Newton Square, PA.

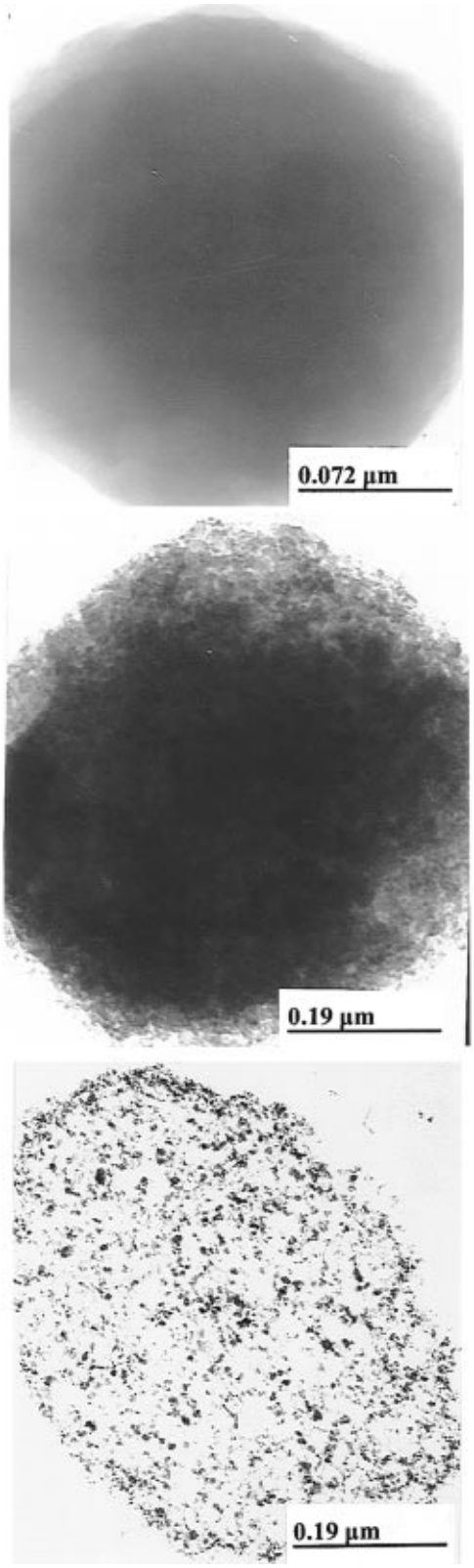

Figure 3. (a, top) Direct-view TEM micrograph of a PEP particle, which is about 0.25 μm in diameter, closer to the lower end of the particle sizes obtained by synthesis in reversed micelles. The relatively smooth outline of the particle suggests an even external surface. (b, middle) Direct-view TEM micrograph of a ferrite−PEP particle synthesized in reversed micelles. The more diffuse outline suggests a rough texture of the external surface. (c, bottom) Cut-section TEM micrograph of a ferrite−PEP particle. The particle may be deformed from its spherical shape due to compressive shear from the diamond cutting knife.

very small volumes, and thermal fluctuations are sufficient to overcome the anisotropy energy barrier, allowing the magnetization to spontaneously reverse direction. As the temperature is significantly lowered to 4.5 K, the sample starts to display some hysteresis with coercivity $H_c \approx 700$ G, as seen in Figure 5b. The presence of low-temperature hysteresis together with the absence of hysteresis at higher temperatures confirms the superparamagnetism of the ferrite−PEP composite. If the sample did not show hysteresis at any temperature, it would be classified as being made up of single-domain particles with the hard axis aligned.[20]

The same trends are seen for the w_0 5 and w_0 10 samples, with hysteresis absent at 100.0 K and present at very low temperatures. Some subtle differences in the shape of the hysteresis loops were present, however. In the w_0 15 sample, the initial slope near the origin is very steep and at very high fields (±50 kG) the magnetization is almost saturated. On the other hand, the w_0 5 and w_0 10 samples display a gradual slope near the origin and the magnetization never quite reaches saturation at very high fields. The slope near the origin, measured as $(dM/dH)_{H=0}$, is 1.06×10^{-3} emu/g G for the w_0 15 sample, and the w_0 5 sample exhibits a much smaller slope of 4.9×10^{-3} emu/g G. The relevant data are summarized in Table 1, which will be referred to as further results are presented. Since the lack of saturation at very high magnetic fields is typical of very small particle sizes,[21] it is very possible that the subtle differences in the shapes of the hysteresis loops might be due to the variation in particle size.

For superparamagnetic particles, the Langevin function[22] describes the relationship between the magnetization at a particular temperature ($M(T)$) and the applied magnetic field (H) according to the expression shown below, where M_S is the saturation magnetization, μ is the magnetic moment of each particle, k is the Boltzmann constant, and T is the absolute temperature:

$$M(T) = M_s\left[\coth\left(\frac{\mu H}{kT}\right) - \frac{kT}{\mu H}\right]$$

The above expression also describes paramagnetism, with μ representing the magnetic moment of a single atom. In the present case however, μ represents a single-domain particle comprised of $>10^5$ atoms, which explains the term "superparamagnetism". As described in a recent article by Yaacob and co-workers,[21] the slope of the magnetization curve near $H = 0$ can be used to estimate the size of the largest particles present in a sample of nonuniform particle sizes. Thus, the largest "magnetic" size of the particles can be related to parameters through the following expression:[21]

$$d_{\mathrm{mag(max)}} = \left[\frac{18kT}{\pi}\frac{(dM/dH)_{H=0}}{\varrho M_S^{\,2}}\right]^{1/3}$$

where ρ is the density of maghemite (5.07 g/cm^3). In

(20) Fuller, M.; Goree, W. S.; Goodman, W. L. In *Magnetite Biomineralization and Magnetoreception in Organisms*, Kisrchvink, J. L., Jones, D. S., MacFadden, B. J., Eds.; Plenum Press: New York, 1985; p 103.

(21) Yaacob, I. I.; Nunes, A. C.; Bose, A.; Shah, D. O. *J. Colloid Interface Sci.* **1995**, *171*, 73.

(22) Cullity, B. D. In *Introduction to Magnetic Materials;* Addison-Wesley: Reading, MA, 1972; p 94.

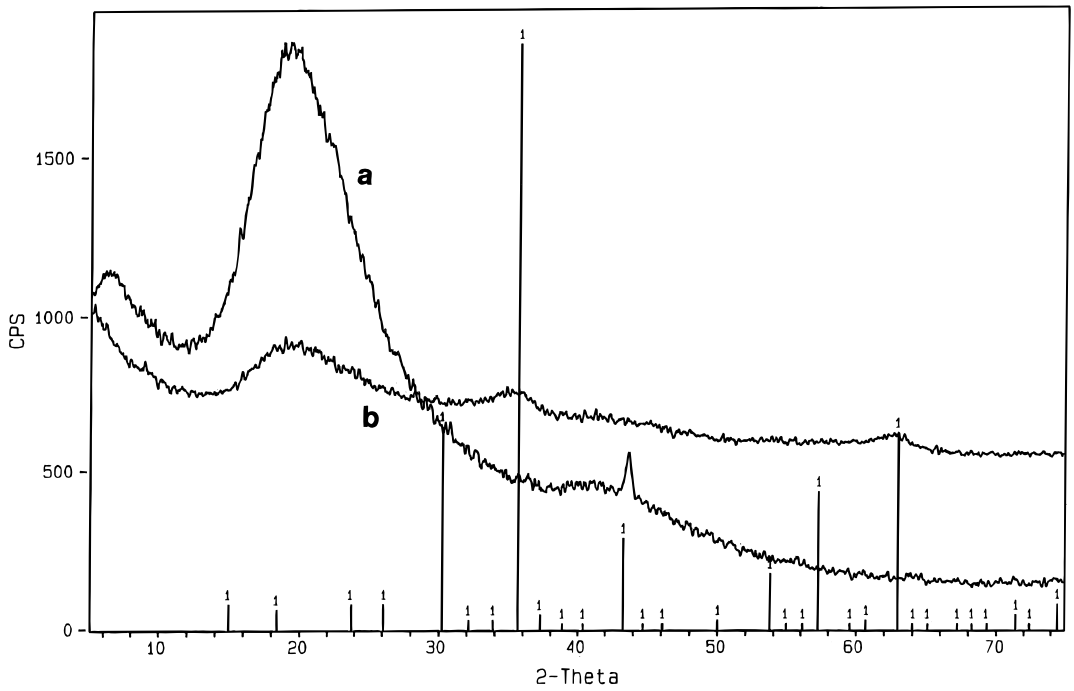

Figure 4. X-ray diffraction pattern for the (a) PEP and (b) ferrite−PEP particles. The vertical lines are the XRD reference for γ-Fe_2O_3 from the ICDD database. The broad peaks which are seen in the ferrite−PEP sample at 35.63° and 62.93° originate from the ferrite particles. Peak broadening due to the extremely small dimensions of the ferrite particles prevents precise identification of the ferrite phase.

our calculations, the limiting slope near the origin was determined from the hysteresis plots by curve-fitting the linear portion of the data. The saturation magnetization for maghemite, $M_S = 76.0$ emu/g, was also used in the calculation.[8] Estimates of $d_{mag(max)}$ show that the "magnetic" size increases as the w_0 of the sample increases. The $d_{mag(max)}$ values corresponding to the samples w_0 5, w_0 10, and w_0 15 are summarized in Table 1 and illustrate a very small magnetic size (0.5−1.5 nm). It is hard to clearly obtain ferrite particle sizes with the TEM resolution available to us, but clusters anywhere between 1 and 10 nm can be observed in the micrograph of Figure 3c. In general, the visually observed particle size is larger than the $d_{mag(max)}$ values; the disparity could perhaps be attributed to the magnetically "dead" layer reported to be present on the surface of magnetic particles.[23] Better agreement may also be obtained by using the saturation magnetization (M_S) corresponding to the true ferrite phase composition rather than just using the M_S of maghemite. The XRD pattern indicates maghemite as the dominant phase, but because of the line broadening at these small particle sizes, the true phase composition is not easily estimated. But the most important result here is the fact that the magnetic size of the superparamagnetic ferrite clusters in the composite can be controlled by simple manipulation of w_0, the water-to-surfactant molar ratio of the micellar solution.

Temperature-dependent dc magnetic susceptibility (χ_{dc}) data for the w_0 15 sample obtained by two different methods are shown in Figure 6. At high temperatures, the field-cooled (FC) and zero-field-cooled (ZFC) magnetization data exhibit the same trend. However, at low temperatures they significantly diverge. The FC curve reaches a plateau and the ZFC curve shows a dramatic decrease in magnetization. From the ZFC data in Figure 6, it is apparent that there is a sharp maximum in the magnetization when plotted as a function of temperature. This maximum is a characteristic of spin glass type materials[24,25] and for the ferrite−PEP composite (w_0 15) studied here, it occurs at 26.0 K. Magnetic particles of very small size are known to mimic some of the properties of spin glass materials and to exhibit blocking temperatures.[26] Going back to the hysteresis loops shown in Figure 5, it is worth noting that the sample exhibits hysteresis at temperatures below 26.0 K, with hysteresis vanishing at higher temperatures. The observation is consistent with the behavior of ultrafine magnetic particles.[27,28]

Magnetic susceptibility measurements (χ_{dc} and χ_{ac}) for many magnetic materials yield the same result because $\chi_{dc} = M/H$ is equal to $\chi_{ac} = dM/dH$ for a well-behaved paramagnet. The spin glass phenomenon is, however, associated with some unusual behavior in the bulk magnetic properties of the materials. The onset of the spin glass state greatly modifies the ability of the electron to follow the applied magnetic field, and the inability is evident through ac-magnetic susceptibility measurements. The magnetic response from the specimen tends to lag behind the oscillating magnetic field if the frequency of the oscillating field is high enough.

(23) Kaiser, R.; Miskolczy, G. *J. Appl. Phys.* **1970**, *41*, 1064.

(24) Zhang, J. H.; Birdwhistell, T. L.; O'Connor, C. J. O. *Solid State Commun.* **1990**, *74*, 443.

(25) O'Connor, C. J. O. In *Research Frontiers in Magnetochemistry*; O'Connor, C. J. O., Ed.; World Scientific Publishing, Inc.: London, 1993; p 109.

(26) Fiorani, D. In *Studies of Magnetic Properties of Fine Particles and Their Relevance to Materials Science*; Dormann, J. L., Fiorani, D., Eds.; Elsevier: Lausanne, 1992; p 135.

(27) McHenry, M. E.; Majetich, S. A.; Artman, J. O.; DeGraef, M.; Staley, S. W. *Phys. Rev. B* **1994**, *49*, 11358.

(28) Brunsman, E. M.; Sutton, R.; Bortz, E.; Kirkpartick, S.; Midelfort, K.; Williams, J.; Smith, P.; McHenry, M. E.; Majetich, S. A.; Artman, J. O.; DeGraef, M.; Staley, S. W. *J. Appl. Phys.* **1994**, *75*, 5882.

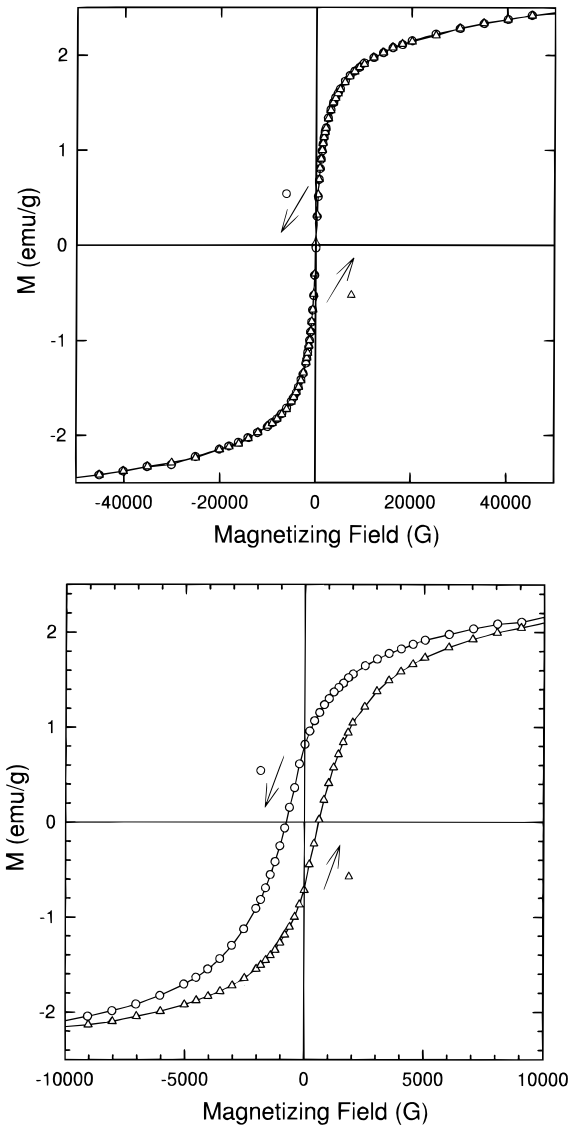

Figure 5. (a, top) Magnetic hysteresis loop for the w_0 15 ferrite−PEP sample at 100.0 K. The lack of hysteresis indicates the composite has superparamagnetic properties. (b, bottom) Magnetic hysteresis loop for the w_0 15 ferrite−PEP sample at 4.5 K. The presence of hysteresis at low temperatures indicates that the ferrite particles undergo a superparamagnetic/single-domain transition.

Table 1. Summary of Key Parameters from Magnetic Measurements

w_0 used in iron oxide synthesis	wt % Fe in composite	$(dM/dH)_{H=0}$ emu/g G	d_{mag}, nm	T_B, K from TRM, IRM data
5	4.03	4.9E−5	0.51	12
10	4.48	1.4E−4	1.05	20
15	5.34	1.06E−3	1.42	27

Recalling that the χ_{ac} experiment is done while oscillating a field of 1.0 G at a frequency of 25 Hz under a static zero field, it is possible through phase-sensitive detection to monitor the in-phase (χ') and out-of-phase (χ'') components of the ac magnetic susceptibility. Figure 7 shows the χ_{ac} data as a function of temperature. The sharp maxima are due to the inability of the spins or particle moments to react to the alternating magnetic field.

One of the frequently performed diagnostic experiments to characterize the spin glass state is the dependence of TRM and IRM on the applied magnetic field.

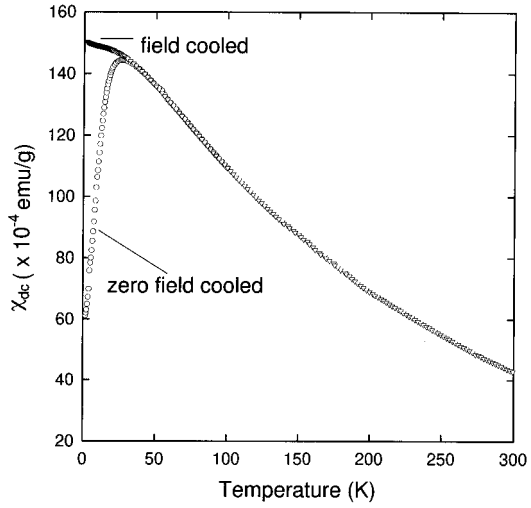

Figure 6. Temperature-dependent field-cooled and zero-field-cooled dc magnetic susceptibility for the w_0 15 ferrite−PEP composite. The experiment was conducted at an applied field of 1 kG. The hump in the zero-field-cooled curve is typical of spin glass materials.

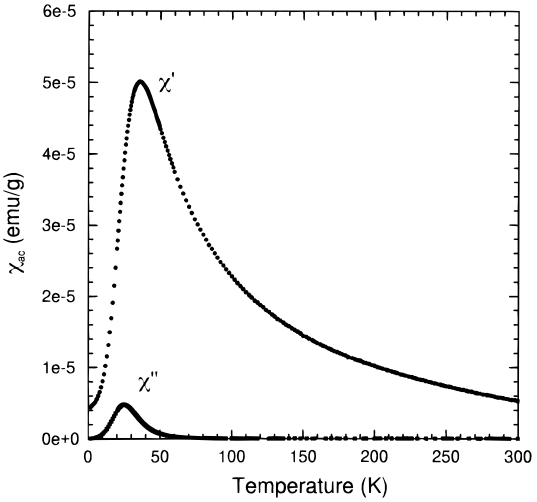

Figure 7. Temperature-dependent ac magnetic susceptibility for the w_0 15 ferrite−PEP composite. The experiment was conducted at static zero field. The maxima in the in-phase (χ') and out-of-phase (χ'') components confirms the spin glass type behavior seen from the χ_{dc} experiments.

For the w_0 5 sample, the TRM and IRM data as a function of field at 4.5 K are shown in Figure 8. The TRM attains a maximum at 3 kG and then slowly decreases and remains essentially invariant above 20 kG. The IRM increases sharply till about 10 kG and eventually reaches a plateau at magnetic fields above 20 kG. The TRM and IRM curves converge at high magnetic fields indicating that the magnetic effects which lead to the blocking of particle moments are destroyed at these large fields. The magnitude of the TRM is always greater than the IRM due to the nature of the experiment. In the TRM experiment, the sample is slowly cooled in the presence of a magnetic field to a temperature below the blocking temperature, and then the field is switched off. The remanent magnetization is later measured after an elapsed time of 300 s. For the IRM experiment, the sample is first cooled below the blocking temperature in zero field, followed by exposure to magnetic field for a specified time of 300 s, turning off the field, and measuring the remanent magnetization after 300 s. During the TRM experiment,

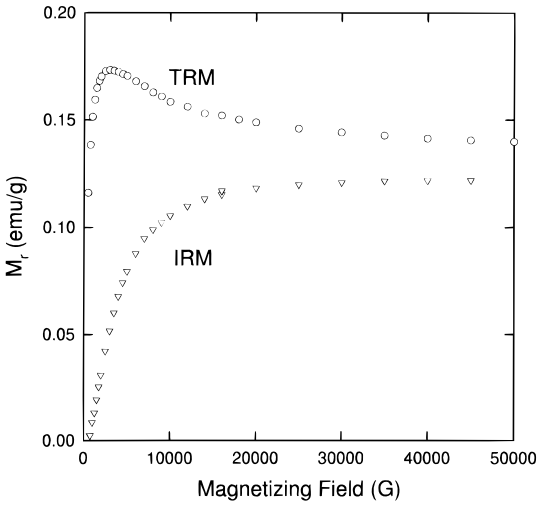

Figure 8. Field-dependent thermal remanent magnetization (TRM) and isothermal remanent magnetization (IRM) plots for the w_0 5 ferrite−PEP composite. The measurements were taken at 4.5 K. The spin glass state is destroyed at high magnetic fields, and the two curves tend to merge.

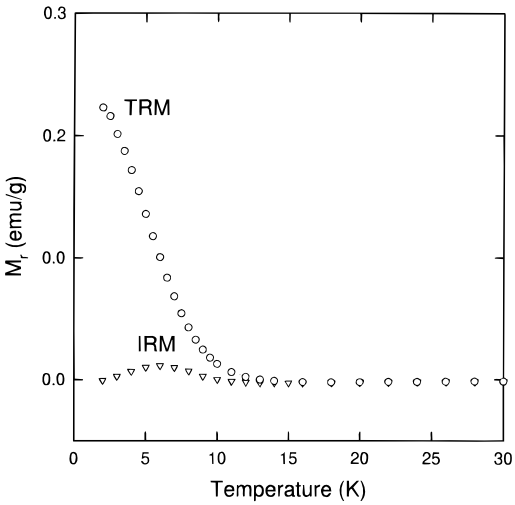

Figure 9. Temperature-dependent thermal remanent magnetization (TRM) and isothermal remanent magnetization (IRM) plots for the w_0 5 ferrite−PEP composite. The measurements were taken at 1 kG. The blocking temperature can be accurately determined from the point of coincidence of the two remanent magnetization curves.

the magnetic moments are frozen in partial alignment with the applied magnetic field when the temperature falls below the freezing temperature, causing the spin glass state. By switching off the field in the spin glass state, the magnetic field is quenched but the spins are still aligned in their frozen state and the sample possesses a resultant moment. Hence, the TRM experiment displays a large remanence compared to the IRM, where the spins are aligned in a random fashion during the transition to the spin glass state since there is no external magnetic field to influence their alignment.

The sensitivity of the TRM and IRM measurements to temperature is illustrated by Figure 9. These measurements provide the most accurate estimation of the blocking temperature, T_B. The remanence obtained by TRM is greatly amplified at low temperatures, and the IRM displays a very minor dependence on temperature. The TRM rapidly decreases as the temperature is increased. The TRM and IRM curves eventually coincide and the remanence goes to zero. The point at which the TRM and IRM measurements coincide gives a very precise estimate of the blocking temperature, which in this case turns out to be 12.0 K for the w_0 5 sample. T_B values of 20.0 and 27.0 K were obtained for the w_0 10 and w_0 15 samples, respectively. Such an elevation in the blocking temperature could be attributed to the increase in the size of the magnetic domains.[29] The increase in particle size with w_0 is confirmed from the d_{mag} analysis.

Conclusions

Ferrite nanoparticles synthesized in the microenvironment of water-in-oil microemulsions have been successfully incorporated into a polymer matrix. The encapsulation of inorganic particles into the polymer is achieved by first synthesizing the ferrites in reversed micelles, followed by the polymerization of *p*-ethylphenol in the same reaction medium. The procedure resembles a ship-in-a-bottle approach to preparing polymer−ferrite composites. The submicron-sized polymer particles when analyzed through ultramicrotoming TEM techniques reveal that the ferrite nanocrystals are uniformly distributed throughout the polymer matrix. Due to their extremely small dimensions, the iron particles entrapped in the polymer are superparamagnetic in nature, as seen by the lack of hysteresis at high temperatures. The composites synthesized exhibit spin glass type behavior with blocking temperatures between 12.0 and 27.0 K. Below the blocking temperature, hysteretic behavior is displayed by the composite, consistent with ultrafine magnetic particle systems. The synthesis of the ferrite−polymer composite can be easily extended to incorporate other inorganic materials of interest into the polymer matrix.

Some potential applications for these composites can be briefly stated. The ability to synthesize the composites as micron and submicron spheres (or clusters) implies an ease in formulating polymeric dispersions for coatings applications. The area of magnetic coatings is a possible application. The surface areas associated with such microspheres indicate application possibilities in separations technologies. For example, antibodies coupled to the polymeric surface may serve as specific receptors and the antibody−antigen complexes could be removed from solution through the application of a magnetic field to recover the complex containing composite particles.[30] Indeed, styrene divinyl benzene−ferrite composites made through the Ugelstad method[31] are the basis of a commerical product used for this purpose. Other applications to drug delivery by magnetically guiding drug-coated composite particles to tumor sites[32] also exist. Medical imaging, ferrofluid technology, information storage, etc., are other potential application areas. Incorporation of other inorganics in the polymer matrix may lead to a wider range of

(29) Towne, W. F.; Gould, J. L. In *Magnetite Biomineralization and Magnetoreception in Organisms*; Kirschvink, J. L., Jones, D. S., MacFadden, B. J. Eds.; Plenum Press: New York, 1985; p 402.
(30) Olsvik, O.; Popovik, T.; Skjerve, E. *Clin. Microbiol. Rev.* **1994**, 43.
(31) Nustad, K.; Danielson, H.; Rieth, A.; Funderud, S.; Lea, T.; Vartdal, F.; Ugelstad, J. In *Microspheres: Medical and Biological Applications*; Rembaum, A., Tökés, Z. A., Eds.; CRC Press: Boca Raton, FL, 1988; p 53.
(32) Sugibayashi, K.; Morimoto, Y. In *Polymeric Nanoparticles and Microspheres*; Guiot, P., Couvreur, P., Eds.; CRC Press: Boca Raton, FL, 1986; p 95.

applications, e.g., photocatalysis with TiO_2 and CdS. It is hoped that some of these applications will be realized.

Acknowledgment. This work was supported by the U. S. Army (Contract DAAK60-93-K-0005) and the National Science Foundation (Grant BCS-9292123). C.J.O. acknowledges support from the Louisiana Educational Quality Support Fund (LEQSF) for the purchase of the SQUID. The authors thank Ms. Zuzana Hruska and Mr. Owen Mills for their help with SEM and TEM and Mr. Pierre Burnside for assistance with the XRD measurements.

CM940485O